An adaptive, non-singular measurement model for angles-only orbit determination and estimation

James E. Hippelheuser
PhD Student, University of Central Florida
Tarek A. Elgohary
Assistant Professor, University of Central Florida

ABSTRACT

Within this work, a new adaptive measurement model is adopted for orbit determination and estimation. The new measurement model revolves around a network of observation nodes that utilizes angle-only line-of-sight measurements produced by a monocular camera. The line-of-sight measurements from each observation node are used to define a pair of orthogonal geometric planes that intersect both the observation node and the target. The intersection of these geometric planes defines the line between each observation node and the target within the inertial frame. This results in three possible combinations of the components of the line-of-sight vector, each of which involves a matrix inversion operation which may introduce singularities. In this work, we introduce an adaptive singularity free measurement model based on maximizing the determinant of the measurement matrix that leads to the optimal condition number. By selecting the line-of-sight components associated with the optimal solution, the measurement model is guaranteed to be singularity free. The new adaptive measurement model is used in an orbit determination framework based on Gaussian least squares differential correction (GLSDC) and an online extended Kalman filter (EKF). A modified version of the Herrick-Gibbs method that incorporates the static form of the measurement model is used as a "warm start" to initiate the estimation scheme. Two scenarios are presented: (1) a small number of observers tracking a single target, and (2) a large constellation of observers tracking a target within a range of orbits. The results show that the adaptive measurement model is capable of performing accurate orbit determination and estimation.

1. INTRODUCTION

The expansion of space flight operations over the last few years has continuously increased the demand for highly accurate orbit determination and estimation methods [37, 25, 28, 3]. As a result of the large and the predicted exponential growth of debris in Earth orbits [2, 20], a dedicated network of observation satellites benefits space situational awareness (SSA) applications. With the expansion of both private and commercial space flight operations, space traffic management (STM) also benefits from having such a network in place [21].

Angles-only measurements have been used primarily for space-based orbit determination [19, 36, 5, 27, 26]. Early uses of angles-only measurements include Gauss and Laplace to perform orbit determination of celestial objects [1, 4]. Recent developments include several iterative methods, e.g. the Double-r method [9] and the Gooding method [13]. In general, IOD is used to provide an initial estimate for other filtering and estimation techniques and some of the more widely used IOD methods are presented in [18]. Accurate orbit determination can also be achieved using nonlinear least squares, e.g. Gauss least squares differential correction (GLSDC), and is capable of incorporating a variety of measurement methods [30]. The number of filtering techniques presented within the literature for Earth-based and space-based measurement models is extensive, but mainly focus on either the extended Kalman filter (EKF) or the unscented Kalman filter (UKF). Several of these works focused on comparing the advantages and disadvantages of the different estimation techniques for various measurement models [30, 24, 29, 6]. The metrics extensively studied within these works include measurements sampling time, the measurement model, the sensitivity towards the initial covariance, the accuracy and the computational time. Results show that the UKF has better convergence characteristics with sparser sampling whereas the EKF has an advantage in computational efficiency [29].

Angles-only measurements of an object is acquired simply by using monocular cameras or telescope [19, 27, 36]. Whereas more complex methods are required for azimuth-elevation angles and range measurements, e.g. LiDAR or

Radar [22, 23, 34]. For angles-only measurements, the line-of-sight measurements have been generally considered as non-observable [35]. Few possible solutions to this problem have been proposed; to include the use of higher order or the full nonlinear relative dynamics in lieu of using the linearized dynamics [5, 19, 27], to offset the measurement device and to include it in the system dynamics [11], to introduce a control input [27, 36, 26, 14, 10], and to introduce a second measurement source where the measurements are expressed in terms of the primary measurements [7, 33, 32].

In this work, a new adaptive measurement model is applied to a network of observation satellites. The measurement model relies on angles-only line-of-sight measurements in the inertial frame of reference. The model uses the concept of intersecting planes [12] to define the line connecting the position of the observation node and the target which results in the estimation of the position and velocity of the target in the inertial frame [15, 16, 17]. The resulting measurement model is not unique and has a singularity, which is avoided by selecting the model associated with the maximum component of the line-of-sight vector. Two space-based orbit determination scenarios are used to evaluate the new measurement model. First, two observation nodes are used in close proximity to track a single target. Then, this is expanded to a full constellation of observers. Within each scenario, the new adaptive measurement model is used first to perform orbit determination utilizing a modified Herrick-Gibbs as a "warm start" to perform GLSDC. Finally, the new adaptive measurement model is incorporated within an EKF framework to perform inertial orbit estimation for both scenarios.

2. AN ADAPTIVE MEASUREMENT MODEL

Each observation node produces two angle measurements, elevation (El) and azimuth (Az), as shown in Fig. 1. From these angle measurements, a line-of-sight unit vector (**LOS**) is created pointing from the observation node to the target in the body frame of the observation node.

$$\mathbf{LOS}_{Obs\rightarrow Tar} = \begin{bmatrix} \cos El \sin Az \\ \cos El \cos Az \\ \sin El \end{bmatrix} \tag{1}$$

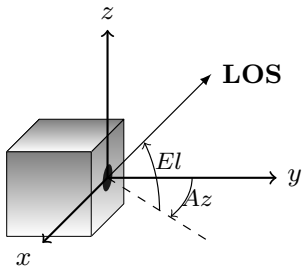

Fig. 1: Angle Measurements

The **LOS** vector is rotated from the body frame to the LVLH frame utilizing the Euler angles roll, pitch, and yaw. With the orbit elements inclination angle, longitude of the ascending node, and true longitude, the **LOS** vector is then rotated from the LVLH frame of the observation node to the ECI frame.

Multiple **LOS** vectors are created from multiple observation nodes and are represented for the K^{th} observer as $\mathbf{LOS}_{ObsK\rightarrow Tar}$. The state vector of the target and the K^{th} observation node are represented as $\mathbf{X}_{Tar}$ and $\mathbf{X}_{ObsK}$, respectively. From the position vector of each observation node, a unit vector is created from the observation node to the origin, $\mathbf{R}_{ObsK\rightarrow O}$.

For each observation node, two orthogonal planes are created that intersect both the observation node and the target as shown in Fig. 2. In order to define the two planes, where each encompasses both the target and the K^{th} observation node, a point on the plane and the normal vector of the plane are required [12]. For both planes, the position of the observation node is used as the point. The normal vector for the first plane is defined as the cross product of the **LOS**, and the position unit vector, $\mathbf{R}_{ObsK\rightarrow O}$

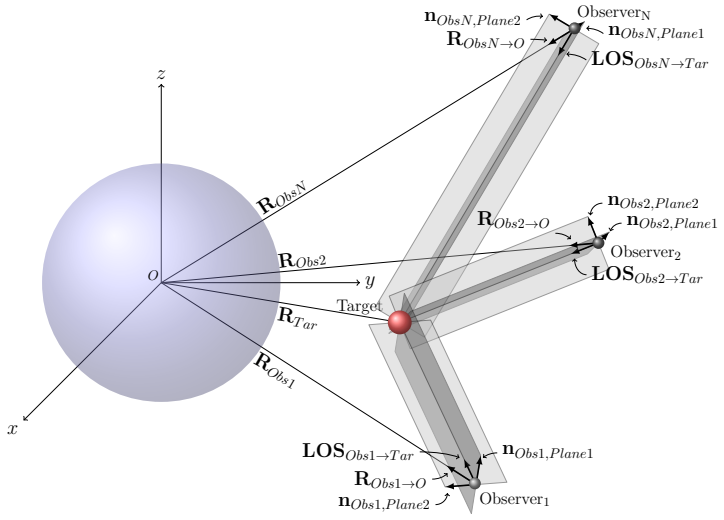

Fig. 2: Geometric plane that intersect both the K^{th} observation node and the target.

$$\mathbf{n}_{ObsK,Plane1} = \mathbf{LOS}_{ObsK\to Tar} \times \mathbf{R}_{ObsK\to O} = \begin{bmatrix} x_{ObsK,Plane1} & y_{ObsK,Plane1} & z_{ObsK,Plane1} \end{bmatrix}^T \tag{2}$$

From Eq. (2), the equation for the first plane, as function of the first normal vector and the K^{th} observer, is

$$x_{ObsK,Plane1}(x - x_{ObsK}) + y_{ObsK,Plane1}(y - y_{ObsK}) + z_{ObsK,Plane1}(z - z_{ObsK}) = 0 \tag{3}$$

For the second plane, the normal vector $\mathbf{n}_{ObsK,Plane2}$ is computed from the cross product of the normal vector of the first plane, $\mathbf{n}_{ObsK,Plane1}$ in Eq. (2), and the **LOS**,

$$\mathbf{n}_{ObsK,Plane2} = \mathbf{n}_{ObsK,Plane1} \times \mathbf{LOS}_{ObsK\to Tar} = \begin{bmatrix} x_{ObsK,Plane2} & y_{ObsK,Plane2} & z_{ObsK,Plane2} \end{bmatrix}^T \tag{4}$$

From Eq. (4), the equation for the second plane, as function of the second normal vector and the K^{th} observer, is

$$x_{ObsK,Plane2}(x - x_{ObsK}) + y_{ObsK,Plane2}(y - y_{ObsK}) + z_{ObsK,Plane2}(z - z_{ObsK}) = 0 \tag{5}$$

The equations of the two orthogonal planes, Eq. (3) and Eq. (5), are expressed in the vector-matrix form

$$\begin{bmatrix} x_{ObsK,Plane1} & y_{ObsK,Plane1} & z_{ObsK,Plane1} \\ x_{ObsK,Plane2} & y_{ObsK,Plane2} & z_{ObsK,Plane2} \end{bmatrix} \begin{bmatrix} (x - x_{ObsK}) & (y - y_{ObsK}) & (z - z_{ObsK}) \end{bmatrix}^T = 0 \tag{6}$$

It is possible to rearrange Eq. (6) into three different equations,

$$\begin{bmatrix} y_{ObsK,Plane1} & z_{ObsK,Plane1} \\ y_{ObsK,Plane2} & z_{ObsK,Plane2} \end{bmatrix}^{-1} \begin{bmatrix} x_{ObsK,Plane1} \\ x_{ObsK,Plane2} \end{bmatrix} = \frac{1}{(x_{ObsK} - x)} \begin{bmatrix} (y - y_{ObsK}) \\ (z - z_{ObsK}) \end{bmatrix} \tag{7a}$$

$$\begin{bmatrix} x_{ObsK,Plane1} & z_{ObsK,Plane1} \\ x_{ObsK,Plane2} & z_{ObsK,Plane2} \end{bmatrix}^{-1} \begin{bmatrix} y_{ObsK,Plane1} \\ y_{ObsK,Plane2} \end{bmatrix} = \frac{1}{(y_{ObsK} - y)} \begin{bmatrix} (x - x_{ObsK}) \\ (z - z_{ObsK}) \end{bmatrix} \tag{7b}$$

$$\begin{bmatrix} x_{ObsK,Plane1} & y_{ObsK,Plane1} \\ x_{ObsK,Plane2} & y_{ObsK,Plane2} \end{bmatrix}^{-1} \begin{bmatrix} z_{ObsK,Plane1} \\ z_{ObsK,Plane2} \end{bmatrix} = \frac{1}{(z_{ObsK} - z)} \begin{bmatrix} (x - x_{ObsK}) \\ (y - y_{ObsK}) \end{bmatrix} \tag{7c}$$

From the definitions of the normal vectors of each plane, Eq. (2) and Eq. (4), **LOS** is expressed as the cross product of $\mathbf{n}_{ObsK,Plane1}$ and $\mathbf{n}_{ObsK,Plane2}$. This simplifies the left hand side of Eq. (7) into components of **LOS**

$$\frac{-1}{x_{ObsK\to Tar}}\begin{bmatrix} y_{ObsK\to Tar} \\ z_{ObsK\to Tar} \end{bmatrix} = \frac{1}{(x_{ObsK}-x)}\begin{bmatrix} (y-y_{ObsK}) \\ (z-z_{ObsK}) \end{bmatrix} \tag{8a}$$

$$\frac{-1}{y_{ObsK\to Tar}}\begin{bmatrix} x_{ObsK\to Tar} \\ z_{ObsK\to Tar} \end{bmatrix} = \frac{1}{(y_{ObsK}-y)}\begin{bmatrix} (x-x_{ObsK}) \\ (z-z_{ObsK}) \end{bmatrix} \tag{8b}$$

$$\frac{-1}{z_{ObsK\to Tar}}\begin{bmatrix} x_{ObsK\to Tar} \\ y_{ObsK\to Tar} \end{bmatrix} = \frac{1}{(z_{ObsK}-z)}\begin{bmatrix} (x-x_{ObsK}) \\ (y-y_{ObsK}) \end{bmatrix} \tag{8c}$$

It is seen in Eq. (8) that the possibility of a singularity exists whenever a component of **LOS** approaches zero. The singularity is avoided by

$$\max\{x_{ObsK\to Tar}, y_{ObsK\to Tar}, z_{ObsK\to Tar}\} \tag{9}$$

When expanded for N observers and replacing $\begin{bmatrix} x & y & z \end{bmatrix}^T$ with the target position, $\mathbf{R}_{Tar} = \begin{bmatrix} x_{Tar} & y_{Tar} & z_{Tar} \end{bmatrix}^T$, it takes on the general form of the nonlinear measurement model

$$\mathbf{y}(t) = \mathbf{h}(\mathbf{x}(t)) \tag{10}$$

and $\mathbf{x}(t)$ represents target's unknown state vector.

3. ORBIT DETERMINATION

3.1 A Modified Herrick-Gibbs Method

The Herrick-Gibbs method requires position measurements for three separate time points and the time difference between each measurement [30]. The modified Herrick-Gibbs method replaces the position measurements with the angle measurements and solving the static problem from Eq. (6).

$$\hat{\mathbf{R}}_{Tar_i} = (A_i^T A_i)^{-1} A_i^T b_i; \quad \text{For } i = 1,2,3 \tag{11}$$

Where,

$$A_i = \begin{bmatrix} x_{Obs1,Plane1_i} & y_{Obs1,Plane1_i} & z_{Obs1,Plane1_i} \\ x_{Obs1,Plane2_i} & y_{Obs1,Plane2_i} & z_{Obs1,Plane2_i} \\ & \vdots & \\ x_{ObsN,Plane1_i} & y_{ObsN,Plane1_i} & z_{ObsN,Plane1_i} \\ x_{ObsN,Plane2_i} & y_{ObsN,Plane2_i} & z_{ObsN,Plane2_i} \end{bmatrix} \tag{12}$$

and

$$b_i = \begin{bmatrix} x_{Obs1,Plane1_i}x_{Obs1_i} + y_{Obs1,Plane1_i}y_{Obs1_i} + z_{Obs1,Plane1_i}z_{Obs1_i} \\ x_{Obs1,Plane2_i}x_{Obs1_i} + y_{Obs1,Plane2_i}y_{Obs1_i} + z_{Obs1,Plane2_i}z_{Obs1_i} \\ \vdots \\ x_{ObsN,Plane1_i}x_{ObsN_i} + y_{ObsN,Plane1_i}y_{ObsN_i} + z_{ObsN,Plane1_i}z_{ObsN_i} \\ x_{ObsN,Plane2_i}x_{ObsN_i} + y_{ObsN,Plane2_i}y_{ObsN_i} + z_{ObsN,Plane2_i}z_{ObsN_i} \end{bmatrix} \tag{13}$$

Once the three positions are determined, the velocity at the second time point is determined as

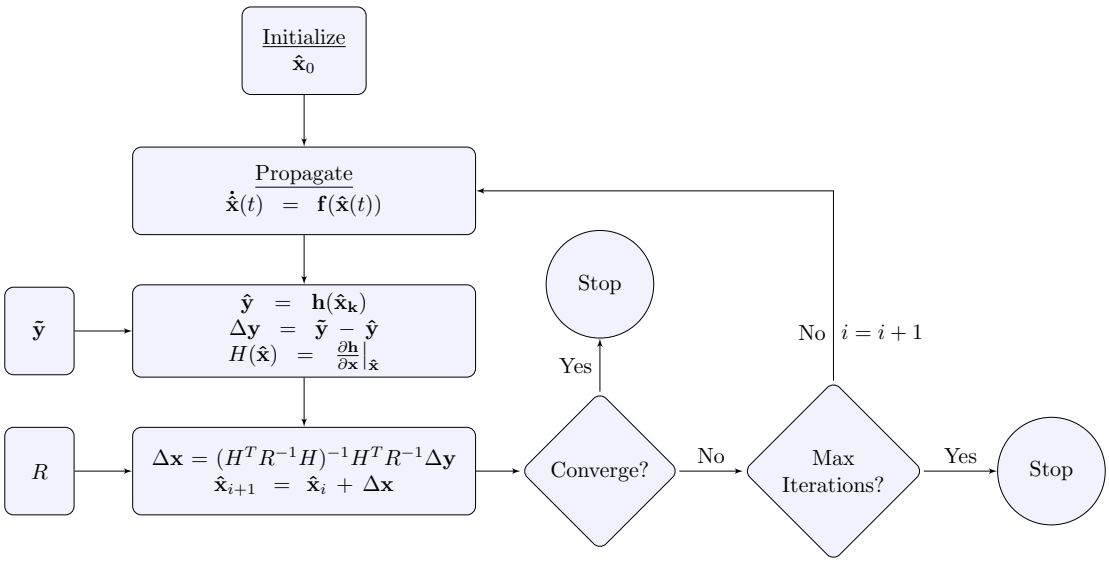

Fig. 3: Gaussian Least Squares Differential Correction

$$\begin{aligned}\hat{\mathbf{V}}_{Tar_2} = &-\Delta t_{23}\left(\frac{1}{\Delta t_{12}\Delta t_{13}} + \frac{\mu}{12\|\mathbf{R}_{Tar_1}\|^3}\right)\hat{\mathbf{R}}_{Tar_1} \\ &+ (\Delta t_{23} - \Delta t_{12})\left(\frac{\Delta t_{23} + \Delta t_{12}}{\Delta t_{23}\Delta t_{12}\Delta t_{13}} + \frac{\mu}{12\|\mathbf{R}_{Tar_2}\|^3}\right)\hat{\mathbf{R}}_{Tar_2} \\ &+ \Delta t_{12}\left(\frac{1}{\Delta t_{23}\Delta t_{13}} + \frac{\mu}{12\|\mathbf{R}_{Tar_3}\|^3}\right)\hat{\mathbf{R}}_{Tar_3}\end{aligned} \tag{14}$$

where

$$\Delta t_{ij} = t_j - t_i \tag{15}$$

The initial state estimate becomes $\hat{\mathbf{x}}_2 = [\hat{\mathbf{R}}_{Tar_2}\ \hat{\mathbf{V}}_{Tar_2}]^T$.

3.2 Gaussian Least Squares Differential Correction

In order to provide a more accurate orbit determination, GLSDC is a iterative method that combines the measurements over time and the dynamics of system [8]. GLSDC is adopted as shown in Fig. 3. A limited number of measurements are taken over a specified time interval. It is initialized using the results from the modified Herrick-Gibbs method. The initial estimation is propagated via the system dynamics over the predetermined time interval. The target dynamics are assumed to follow the Keplerian two-body motion given in the Cartesian ECI frame by

$$\dot{\hat{\mathbf{x}}} = \mathbf{f}(\hat{\mathbf{X}}_{Tar}(t)) = \begin{bmatrix} \hat{\mathbf{V}}_{Tar} \\ -\frac{\mu}{\|\hat{\mathbf{R}}_{Tar}\|^3}\hat{\mathbf{R}}_{Tar} \end{bmatrix} \tag{16}$$

The measurements are then compared to the estimated measurements. The measurements are

$$\tilde{\mathbf{y}} = \begin{cases} \frac{-1}{x_{ObsK\to Tar}} \begin{bmatrix} y_{ObsK\to Tar} \\ z_{ObsK\to Tar} \end{bmatrix} & \text{if } x_{ObsK\to Tar} \text{ is max} \\ \frac{-1}{y_{ObsK\to Tar}} \begin{bmatrix} x_{ObsK\to Tar} \\ z_{ObsK\to Tar} \end{bmatrix} & \text{if } y_{ObsK\to Tar} \text{ is max} \\ \frac{-1}{z_{ObsK\to Tar}} \begin{bmatrix} x_{ObsK\to Tar} \\ y_{ObsK\to Tar} \end{bmatrix} & \text{if } z_{ObsK\to Tar} \text{ is max} \end{cases} \tag{17}$$

and the estimated measurements are

$$\mathbf{h}(\hat{\mathbf{x}}) = \begin{cases} \frac{1}{(x_{ObsK} - \hat{x}_{Tar})} \begin{bmatrix} (\hat{y}_{Tar} - y_{ObsK}) \\ (\hat{z}_{Tar} - z_{ObsK}) \end{bmatrix} & \text{if } x_{ObsK\to Tar} \text{ is max} \\ \frac{1}{(y_{ObsK} - \hat{y}_{Tar})} \begin{bmatrix} (\hat{x}_{Tar} - x_{ObsK}) \\ (\hat{z}_{Tar} - z_{ObsK}) \end{bmatrix} & \text{if } y_{ObsK\to Tar} \text{ is max} \\ \frac{1}{(z_{ObsK} - \hat{z}_{Tar})} \begin{bmatrix} (\hat{x}_{Tar} - x_{ObsK}) \\ (\hat{y}_{Tar} - y_{ObsK}) \end{bmatrix} & \text{if } z_{ObsK\to Tar} \text{ is max} \end{cases} \tag{18}$$

Using the Jacobian of the estimated measurements and the measurement covariance R provided in [15, 16], the estimated states are updated. The Jacobian of the estimated measurements is

$$H(\hat{\mathbf{x}}) = \begin{cases} \begin{bmatrix} \frac{(\hat{y}_{Tar_k} - y_{Obs1_k})}{(x_{Obs1_k} - \hat{x}_{Tar_k})^2} & \frac{1}{(x_{Obs1_k} - \hat{x}_{Tar_k})} & 0 & 0 & 0 & 0 \\ \frac{(\hat{z}_{Tar_k} - z_{Obs1_k})}{(x_{Obs1_k} - \hat{x}_{Tar_k})^2} & 0 & \frac{1}{(x_{Obs1_k} - \hat{x}_{Tar_k})} & 0 & 0 & 0 \end{bmatrix} & \text{if } x_{ObsK\to Tar} \text{ is max} \\ \begin{bmatrix} \frac{1}{(y_{Obs1_k} - \hat{y}_{Tar_k})} & \frac{(\hat{x}_{Tar_k} - x_{Obs1_k})}{(y_{Obs1_k} - \hat{y}_{Tar_k})^2} & 0 & 0 & 0 & 0 \\ 0 & \frac{(\hat{z}_{Tar_k} - z_{Obs1_k})}{(y_{Obs1_k} - \hat{y}_{Tar_k})^2} & \frac{1}{(y_{Obs1_k} - \hat{y}_{Tar_k})} & 0 & 0 & 0 \end{bmatrix} & \text{if } y_{ObsK\to Tar} \text{ is max} \\ \begin{bmatrix} \frac{1}{(z_{Obs1_k} - \hat{z}_{Tar_k})} & 0 & \frac{(\hat{x}_{Tar_k} - x_{Obs1_k})}{(z_{Obs1_k} - \hat{z}_{Tar_k})^2} & 0 & 0 & 0 \\ 0 & \frac{1}{(z_{Obs1_k} - \hat{z}_{Tar_k})} & \frac{(\hat{y}_{Tar_k} - y_{Obs1_k})}{(z_{Obs1_k} - \hat{z}_{Tar_k})^2} & 0 & 0 & 0 \end{bmatrix} & \text{if } z_{ObsK\to Tar} \text{ is max} \end{cases} \tag{19}$$

If the difference between the previous iteration and the current iteration is less than a a predetermined threshold, it is considered converged and the current estimation is the solution. If it has not converged, it starts another iteration. If the maximum number of iterations is reached, then the most recent estimation is considered the solution.

3.3 Extended Kalman Filter

For continuous orbit estimation of the target, EKF is adopted [8] as shown in Fig. 4. As with GLSDC, the state estimate is initialized with the results from the modified Herrick-Gibbs method. The state covariance is initialized as $P_0^- = \text{diag}(10^8)$. The gain, as a function of the measurements, Eq. (17), estimated measurements, Eq. (18), estimated measurement Jacobian Eq. (19), R, estimated sates, and state P, is used to update both the state estimate and the state covariance. The state estimate and state covariance are then propagated to the next time step. The target dynamics are assumed to follow the Keplerian two-body motion given in the Cartesian ECI frame, Eq. (16). The Jacobian of the dynamics evaluated at the estimate, $F(\hat{\mathbf{x}})$, is written as,

$$\begin{aligned} F(\hat{\mathbf{X}}_{Tar}(t)) &= \left.\frac{\partial \mathbf{f}}{\partial \mathbf{x}}\right|_{\hat{\mathbf{X}}_{Tar}(t)} \\ &= \begin{bmatrix} 0_{3\times 3} & I_{3\times 3} \\ F_{21}(\hat{\mathbf{X}}_{Tar}) & 0_{3\times 3} \end{bmatrix} \end{aligned} \tag{20}$$

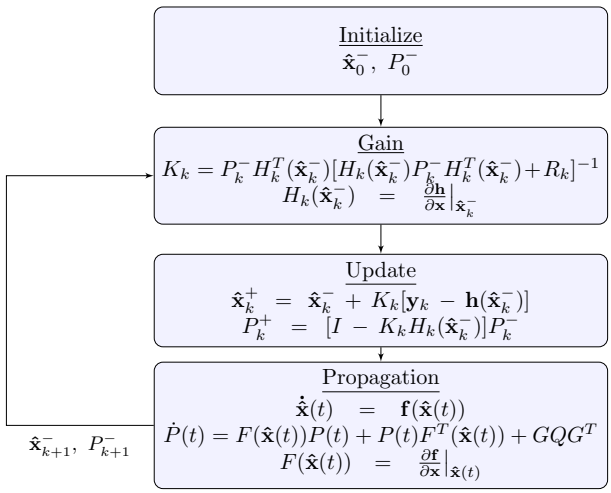

Fig. 4: Continuous-Discrete Extended Kalman Filter

where

$$F_{21}(\hat{\mathbf{X}}_{Tar}) = \frac{\mu}{\|\hat{\mathbf{R}}_{Tar}\|^5}\begin{bmatrix} 3\hat{x}_{Tar}^2 - \|\hat{\mathbf{R}}_{Tar}\|^2 & 3\hat{x}_{Tar}\hat{y}_{Tar} & 3\hat{x}_{Tar}\hat{z}_{Tar} \\ 3\hat{x}_{Tar}\hat{y}_{Tar} & 3\hat{y}_{Tar}^2 - \|\hat{\mathbf{R}}_{Tar}\|^2 & 3\hat{y}_{Tar}\hat{z}_{Tar} \\ 3\hat{x}_{Tar}\hat{z}_{Tar} & 3\hat{y}_{Tar}\hat{z}_{Tar} & 3\hat{z}_{Tar}^2 - \|\hat{\mathbf{R}}_{Tar}\|^2 \end{bmatrix} \tag{21}$$

4. RESULTS

To evaluate each method for orbit determination, two scenarios are considered using the modified Herrick Gibbs method, GLSDC, and EKF. The first set of scenarios involve a small formation of two observers tracking a single target in close proximity. The second set of scenarios involve a large, uniform constellation of observers tracking a single target.

For each approach, the estimation error, $\mathbf{x}_e$, is calculated as the difference between the true states and the estimated states, $\mathbf{x}_e = \mathbf{x}_k - \hat{\mathbf{x}}_k$. The total accuracy of the EKF is determined using the root mean square error (RMSE) as shown in Eq. (22).

$$RMSE = \sqrt{\frac{1}{N}\sum_{1}^{N}\mathbf{x}_e^2} \tag{22}$$

4.1 Small Formation of Observers

The initial scenario involves two observers and a single target, shown in Table 1. First, the first three measurements are used in the modified Herrick-Gibbs method to provide an initial approximation. Then, GLSDC is used to perform an iterative solution for the initial state estimate, relying on the first 21 measurements. Finally, the EKF is used to provide a continuous estimate of the orbit states. For all methods the time-step is 0.5 s.

Table 1: Orbit elements for the target and observation nodes.

	a (km)	e	i (deg)	Ω (deg)	ω (deg)	M_0 (deg)
Target	7000.0	0	25.0	0	N/A	80.0
Observer 1	7000.0	0	25.2	0	N/A	79.6
Observer 2	7000.0	0	25.2	0	N/A	80.4

The initial approximation using the modified Herrick-Gibbs method results in a normalized position error of 51.501 m and a normalized velocity error of 47.859 m/s. For GLSDC, the convergence criteria is $\Delta\mathbf{x} < 10^{-10}$ and the maximum number of iteration is 100. It converges after 15 iterations and results in a normalized position error of 9.328 m and normalized velocity error of 0.240 m/s.

The EKF is applied with a final time of $t_f = 1500$ s. Initially the measurement model is fixed throughout the simulation, specifically Eq. (8c). This results in a singularity at approximately 900 s from one of the observers. The singularity results in poor/divergent performance of the filter, Fig. 5. While a solution previously demonstrated [17, 16, 15] involves the temporary removal of the observation node based on a threshold to avoid the singularity. For this scenario, that requires the temporary removal of both observers because only using one observer is non-observable. The new approach is to use the adaptive measurement model, from Fig. 6 it is seen to show excellent performance. The resulting RMSE for position and velocity is 4.608 m and 0.665 m/s,m respectively.

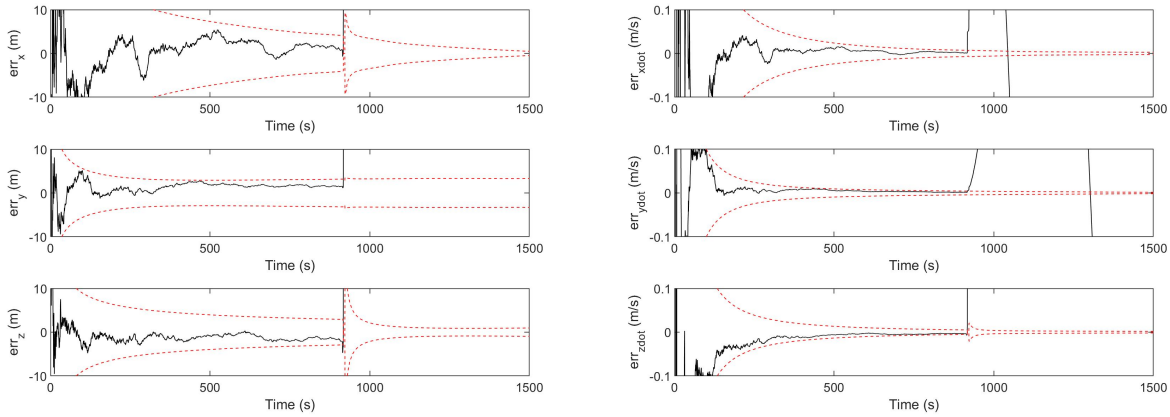

(a) (b)

Fig. 5: Position (a) and Velocity (b) error (black) and $\mathbf{3}\sigma$ bounds (red) using all observers with a fixed measurement model.

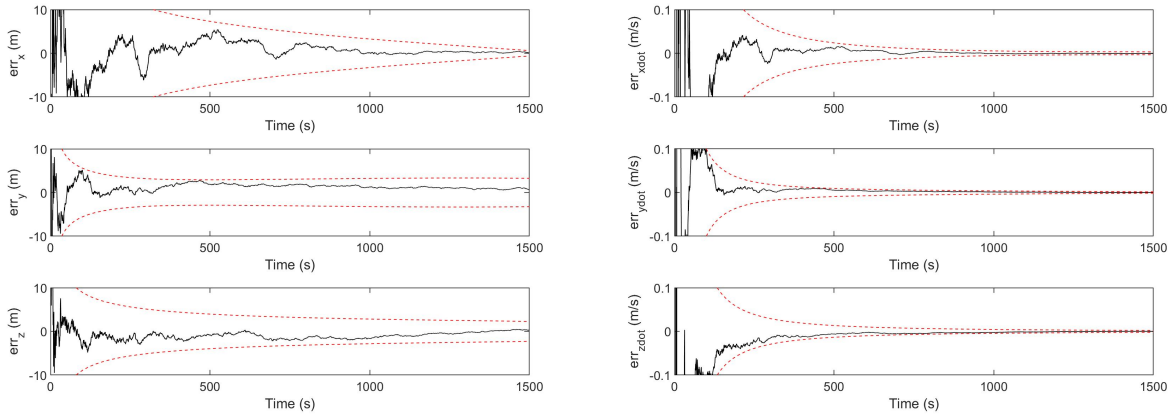

(a) (b)

Fig. 6: Position (a) and Velocity (b) error (black) and $\mathbf{3}\sigma$ bounds (red) using all observers with an adaptive measurement model.

4.2 Large Constellation of Observers

The small formation of two observers is expanded to a full constellation. The observers are organized in a simple Walker Constellation [31]. The elements of the Walker Constellation are $50^\circ : 1296/36/0$, or 1296 satellites evenly

distributed over 36 orbit planes, resulting in 36 satellites per orbit plane. Each orbit plane is evenly distributed every 10° along the longitude of the ascending node and each satellite is evenly distributed every 10° of mean anomaly within each orbit plane. All orbits are circular with a radius of 6800 km and an inclination angle of 50°. Three targets in different orbits are used, shown in Table 2. The orbits were selected with varying inclination angles and with on orbit in retrograde. The maximum sensor range of each observer is limited to 600 km and Earth obstruction is taken into account [15, 16, 29].

Table 2: Orbit elements for the separate target nodes.

	a (km)	e	i (deg)	Ω (deg)	ω (deg)	M_0 (deg)
Target 1	6750.0	0	28.5	0	N/A	-10.0
Target 2	6750.0	0	20.0	0	N/A	15.0
Target 3	6750.0	0	30.0	0	N/A	135.0

The normalized error results for the modified Herrick-Gibbs method are shown in Table 3. For the GLSDC method, number of measurements used is 21. The convergence criteria and max iteration are the same as before, $\Delta\mathbf{x} < 10^{-10}$ and 100, respectively. The required number of iterations and resulting normalized error using GLSDC is shown in Table 4.

Table 3: Modified Herrick-Gibbs error results.

	Pos. Error (m)	Vel. Error (m/s)
Target 1	263.600	997.010
Target 2	331.252	439.885
Target 3	122.479	483.235

Table 4: GLSDC error results.

	Num. Iterations	Pos. Error (m)	Vel. Error (m/s)
Target 1	18	172.901	20.985
Target 2	10	78.452	26.866
Target 3	48	101.276	18.286

For the three targets, the EKF is applied with a final time of $t_f = 5500$ s. The inclusion of the adaptive measurement model shows that error converges for all three targets, Fig. 7. The resulting RMSE for position and velocity are shown in Table 5.

Table 5: EKF error results.

	Pos. RMSE (m)	Vel. RMSE (m/s)
Target 1	26.170	16.856
Target 2	16.875	10.500
Target 3	35.424	16.306

5. CONCLUSION

In this paper, a new adaptive measurement model that relies only on angles-only line-of-sight measurements is presented. The new measurement model is specifically designed for a multiple observation node framework, either a small formation or a large constellation, to provide initial orbit determination and estimation. When used within the modified Herrick-Gibbs method, the results are less then ideal. However, the modified Herrick-Gibbs method is simple to implement and provides an excellent "warm start" for other iterative and sequential methods. The results from GLSDC shows that the adaptive measurement model can preform accurate initial orbit determination. Excellent results are achieved using EKF, converging to an error of a few meters quickly. Moving forward, the portability of the measurement model to possibly be combined with heterogeneous measurements will be explored. Also, because the

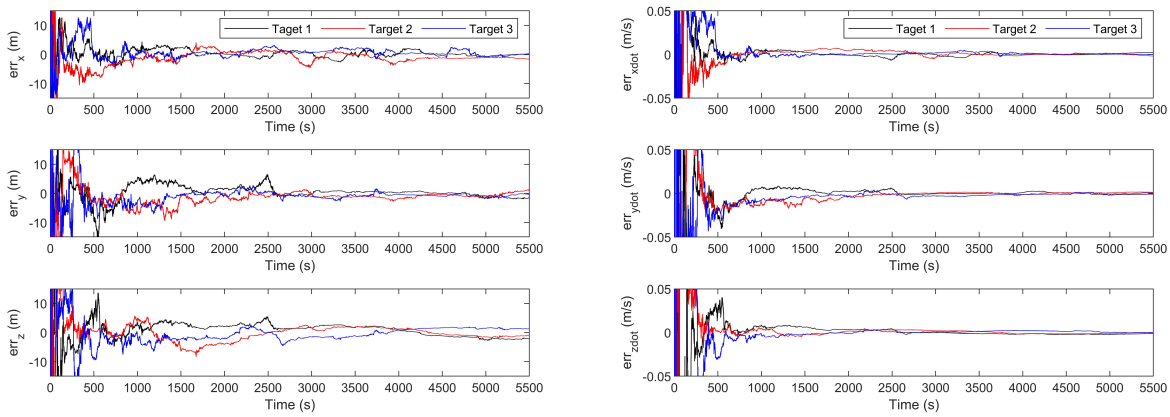

(a) (b)

Fig. 7: Position (a) and Velocity (b) error (black) using a constellation of observers with an adaptive measurement model.

measurement model is in the inertial frame, it has the potential to be used for providing SSA and STM for Cislunar space.

6. REFERENCES

[1] JD Anderson. Theory of orbit determination. part i: classical methods. *Jet Propulsion Laboratory Technical Report*, (32-497), 1963.

[2] Phillip D Anz-Meador. Orbital debris quarterly news volume 23, issues 1 & 2. 2019.

[3] William H Blume. Deep impact: mission design approach for a new discovery mission. *Acta Astronautica*, 52(2-6):105–110, 2003.

[4] Richard L Branham. Laplacian orbit determination and differential corrections. *Celestial Mechanics and Dynamical Astronomy*, 93(1-4):53–68, 2005.

[5] Eric A Butcher, Jingwei Wang, and T Alan Lovell. On Kalman filtering and observability in nonlinear sequential relative orbit estimation. *Journal of Guidance, Control, and Dynamics*, 40(9):2167–2182, 2017.

[6] Huimin Chen, Genshe Chen, Erik Blasch, and Khanh Pham. Comparison of several space target tracking filters. In *Sensors and Systems for Space Applications III*, volume 7330, page 73300I. International Society for Optics and Photonics, 2009.

[7] Tong Chen and Shijie Xu. Double line-of-sight measuring relative navigation for spacecraft autonomous rendezvous. *Acta Astronautica*, 67(1-2):122–134, 2010.

[8] John L Crassidis and John L Junkins. *Optimal estimation of dynamic systems*, pages 184–189. Chapman and Hall/CRC, 2011.

[9] Pedro Ramon Escobal. Methods of orbit determination. *New York: Wiley, 1965*, 1965.

[10] Francisco J Franquiz, Josué D Muñoz, Bogdan Udrea, and Mark J Balas. Optimal range observability maneuvers of a spacecraft formation using angles-only navigation. *Acta Astronautica*, 153:337–348, 2018.

[11] David K Geller and Itzik Klein. Angles-only navigation state observability during orbital proximity operations. *Journal of Guidance, Control, and Dynamics*, 37(6):1976–1983, 2014.

[12] W. Gellert, S. Gottwald, M. Hellwich, H. Kästner, and H. Küstner. *Analytic geometry of space*, pages 530–547. Springer Netherlands, Dordrecht, 1975.

[13] RH Gooding. A new procedure for the solution of the classical problem of minimal orbit determination from three lines of sight. *Celestial Mechanics and Dynamical Astronomy*, 66(4):387–423, 1996.

[14] Jonathan Grzymisch and Walter Fichter. Analytic optimal observability maneuvers for in-orbit bearings-only rendezvous. *Journal of Guidance, Control, and Dynamics*, 37(5):1658–1664, 2014.

[15] James Hippelheuser. Inertial orbit estimation using multiple space based observers: A new measurement model. 2020.

[16] James Hippelheuser and Tarek A Elgohary. Inertial space-based orbit estimation: A new measurement model for multiple observers. *Acta Astronautica*, 2020.
[17] James E Hippelheuser and Tarek A Elgohary. New geometric approach for multi node space-based orbit estimation. In *2nd IAA Conference on Space Situational Awareness*. IAA-ICSSA-20-00-19, 2020.
[18] Reza Raymond Karimi and Daniele Mortari. A performance based comparison of angle-only initial orbit determination methods. *Advances in Astronautical Sciences, AAS/AIAA, Hilton Head Island, South Carolina*, 150:1793–1809, 2013.
[19] Evan Kaufman, T Alan Lovell, and Taeyoung Lee. Nonlinear observability for relative orbit determination with angles-only measurements. *The Journal of the Astronautical Sciences*, 63(1):60–80, 2016.
[20] Donald J Kessler, Nicholas L Johnson, JC Liou, and Mark Matney. The Kessler syndrome: implications to future space operations. *Advances in the Astronautical Sciences*, 137(8):2010, 2010.
[21] Theodore J Muelhaupt, Marlon E Sorge, Jamie Morin, and Robert S Wilson. Space traffic management in the new space era. *Journal of Space Safety Engineering*, 6(2):80–87, 2019.
[22] Roberto Opromolla, Giancarmine Fasano, Giancarlo Rufino, and Michele Grassi. Uncooperative pose estimation with a LIDAR-based system. *Acta Astronautica*, 110:287–297, 2015.
[23] MN Quinn, V Jukna, T Ebisuzaki, I Dicaire, R Soulard, L Summerer, A Couairon, and G Mourou. Space-based application of the CAN laser to LIDAR and orbital debris remediation. *The European Physical Journal Special Topics*, 224(13):2645–2655, 2015.
[24] JR Raol and NK Sinha. On the orbit determination problem. *IEEE Transactions on Aerospace and Electronic Systems*, (3):274–291, 1985.
[25] Brent Sherwood, David B Smith, Ron Greeley, W Whittaker, Gordon R Woodcock, Gregg Barton, David W Pearson, and William Siegfried. Mars sample return: Architecture and mission design. In *Proceedings, IEEE Aerospace Conference*, volume 2, pages 2–536. IEEE, 2002.
[26] Joshua Sullivan and Simone D'Amico. Adaptive filtering for maneuver-free angles-only navigation in eccentric orbits. In *27th AAS/AIAA Space Flight Mechanics Conference*, 2017.
[27] Joshua Sullivan, A Koenig, and Simone D'Amico. Improved maneuver-free approach to angles-only navigation for space rendezvous. In *26th AAS/AIAA Space Flight Mechanics Meeting, Napa, CA*, 2016.
[28] Lorenzo Tarabini, Jesús Gil, Fernando Gandia, Miguel Ángel Molina, Juan Manuel Del Cura, and Guillermo Ortega. Ground guided CX-OLEV rendez-vous with uncooperative geostationary satellite. *Acta Astronautica*, 61(1-6):312–325, 2007.
[29] Bruno OS Teixeira, Mario A Santillo, R Scott Erwin, and Dennis S Bernstein. Spacecraft tracking using sampled-data Kalman filters. *IEEE Control Systems Magazine*, 28(4):78–94, 2008.
[30] David A Vallado. *Fundamentals of astrodynamics and applications*, volume 12. Springer Science & Business Media, 2001.
[31] John G Walker. Satellite constellations. *Journal of the British Interplanetary Society*, 37:559–572, 1984.
[32] Hui Wang, Xiangyi Zhang, Qingrui Zhou, and Yong Li. Autonomous navigation of non-cooperative target based on multiple line-of-sight. In *2017 36th Chinese Control Conference (CCC)*, pages 6276–6280. IEEE, 2017.
[33] Kai Wang, Tong Chen, and Shi-Jie Xu. A method of double line-of-sight measurement relative navigation. *Acta Aeronautica et Aeronautica Sinica*, 32(6):1084–1091, 2011.
[34] Yang Wang and Qianqian Wang. The application of LIDAR in detecting space debris. In *2008 International Conference on Optical Instruments and Technology: Optoelectronic Measurement Technology and Applications*, volume 7160, page 71601S. International Society for Optics and Photonics, 2009.
[35] David C Woffinden and David K Geller. Observability criteria for angles-only navigation. *IEEE Transactions on Aerospace and Electronic Systems*, 45(3):1194–1208, 2009.
[36] David C Woffinden and David K Geller. Optimal orbital rendezvous maneuvering for angles-only navigation. *Journal of guidance, control, and dynamics*, 32(4):1382–1387, 2009.
[37] Douglas Zimpfer, Peter Kachmar, and Seamus Tuohy. Autonomous rendezvous, capture and in-space assembly: past, present and future. In *1st Space exploration conference: continuing the voyage of discovery*, page 2523, 2005.